

Fighting topological freezing in the two-dimensional CP^{N-1} model ^{*}

Martin Hasenbusch

¹*Institut für Physik, Humboldt-Universität zu Berlin, Newtonstr. 15, 12489 Berlin, Germany*

Abstract. We perform Monte Carlo simulations of the CP^{N-1} model on the square lattice for $N = 10, 21$, and 41 . Our focus is on the severe slowing down related to instantons. To fight this problem we employ open boundary conditions as proposed by Lüscher and Schaefer for lattice QCD. Furthermore we test the efficiency of parallel tempering of a line defect. Our results for open boundary conditions are consistent with the expectation that topological freezing is avoided, while autocorrelation times are still large. The results obtained with parallel tempering are encouraging.

1 Introduction

The CP^{N-1} model shares fundamental properties such as asymptotic freedom and confinement with QCD. Therefore it serves as a toy model of QCD. It has been shown [1, 2] that the model has a non-trivial vacuum structure with stable instanton solutions. It turned out that these topological objects pose a particular problem in the simulation of the lattice CP^{N-1} model, similar to lattice QCD.

On the torus, in the continuum limit, the configuration space is decomposed into sectors that are characterized by their topological charge. At finite lattice spacing, the free energy barriers between such sectors increase as the lattice spacing decreases. For Markov chain Monte Carlo algorithms that walk in a quasi continuous fashion through configuration space this means that they become essentially non-ergodic and slowing down becomes dramatic. Numerical results are compatible with an increase of autocorrelation times that is exponential in the inverse lattice spacing. In the case of the CP^{N-1} model this is numerically verified, for example, in refs. [3–5]. Modelling the autocorrelation times with a more conventional power law Ansatz, large powers are needed to fit the data. From a practical point of view, the consequence is that it becomes virtually impossible to access lattice spacings below a certain threshold. The numerical studies show that in the case of the CP^{N-1} model the problem becomes worse with increasing N . Since it is much less expensive to simulate the two-dimensional model than lattice QCD, it is a good test bed for new ideas and algorithms that could overcome the severe slowing down of the topological modes. For example simulated tempering [6] has been studied in ref. [7] with moderate success. More recently, “trivializing maps in the Hybrid Monte Carlo algorithm” [8] or the “Metadynamics” method [9] have been tested.

A very principle solution of the problem had been suggested in ref. [10]. By abandoning periodic boundary conditions in one of the directions in favour of open ones, barriers between the topological

^{*}Talk given at the 35th International Symposium on Lattice Field Theory, 18 - 24 June 2017, Granada, Spain.

sectors are abolished. The proposal has been further tested [11, 12] and adopted in large scale simulations of lattice QCD with dynamical fermions [13, 14]. Here we shall probe in detail how open boundary conditions effect the slowing down in the case of the CP^{N-1} model. Since the CP^{N-1} model is much cheaper to simulate than lattice QCD, a larger range of lattice spacings can be studied and autocorrelation functions can be computed more accurately.

Furthermore, we shall explore parallel tempering [15–18] as a solution to our problem. Parallel tempering is a well established approach in statistical physics to overcome effective non-ergodicity due to a ragged free energy landscape. The idea of parallel tempering and similar methods is to enlarge the configuration space such that the hills can be easily by-passed. A prototype problem is the study of spin-glasses, where parallel tempering is mandatory. For recent work see for example ref. [19]. Typically a global parameter such as the temperature or an external field is used as parameter of the tempering. Here instead, we shall discuss a line defect.

Finally we like to mention that for the CP^{N-1} model dual formulations can be found. These can be simulated by using the worm algorithm [20, 21]. In these dual formulations there are no topological sectors and hence severe slowing down does not occur in the simulation.

2 The model

We consider a square lattice with sites $x = (x_0, x_1)$, where $x_i \in \{0, 1, 2, \dots, L_i - 1\}$. The lattice spacing is set to $a = 1$. This means that we trade a decreasing lattice spacing for an increasing correlation length. The action is

$$S = -\beta N \sum_{x,\mu} \left(\bar{z}_{x+\hat{\mu}} z_x \lambda_{x,\mu} + z_{x+\hat{\mu}} \bar{z}_x \bar{\lambda}_{x,\mu} - 2 \right), \quad (1)$$

where z_x is a complex N -component vector with $z_x \bar{z}_x = 1$ and $\lambda_{x,\mu}$ is a complex number with $\lambda_{x,\mu} \bar{\lambda}_{x,\mu} = 1$. The gauge fields live on the links, which are denoted by x, μ , where $\mu \in \{0, 1\}$ gives the direction and $\hat{\mu}$ is a unit vector in μ -direction. In 1-direction we always consider periodic boundary conditions. In 0-direction either open or periodic boundary conditions are considered. We implement open boundary conditions in a crude way, simply setting $\beta = 0$ for the links that connect $x_0 = L_0 - 1$ and $x_0 = 0$.

2.1 The observables

We measure the energy, the magnetic susceptibility, the second moment and the exponential correlation length. For the definition of these quantities see for example ref. [3] or section II A of ref. [22]. Our main focus is on the topology of the field. Motivated by eq. (33) of ref. [3] we define the plaquette angle

$$\theta_{plaq,x} = \theta_{x,\mu} + \theta_{x+\hat{\mu},\nu} - \theta_{x+\hat{\nu},\mu} - \theta_{x,\nu} - 2n\pi, \quad \mu \neq \nu, \quad (2)$$

where $\theta_{x,\mu} = \arg\{\bar{z}_x z_{x+\hat{\mu}}\}$ and the integer n is chosen such that $-\pi < \theta_{plaq,x} \leq \pi$. We define the topological charge density $q_x = \frac{1}{2\pi} \theta_{plaq,x}$. The topological charge on the lattice with periodic boundary conditions is defined by

$$Q = \sum_x q_x = \frac{1}{2\pi} \sum_x \theta_{plaq,x}. \quad (3)$$

The topological susceptibility is then given by

$$\chi_t = \frac{1}{V} \langle Q^2 \rangle = \frac{1}{L_0 L_1} \left\langle \sum_{xy} q_x q_y \right\rangle = \frac{1}{L_0 L_1} \left\langle \sum_{x_0 x_1} q_{x_0, x_1} \sum_{y_0 y_1} q_{y_0 y_1} \right\rangle = \frac{1}{L_0} \left\langle \sum_{x_0} \tilde{q}_{x_0} \sum_{y_0} \tilde{q}_{y_0} \right\rangle, \quad (4)$$

where we define $\tilde{q}_{x_0} = \frac{1}{\sqrt{L_1}} \sum_{x_1} q_{x_0, x_1}$. Note that the definition of the topological charge given in ref. [23] and (3) are not equivalent at finite lattice spacing. We checked numerically that the difference between the two definitions decreases quickly with increasing β . Also cooling of the configurations strongly reduces the difference.

On the lattice with periodic boundary conditions, Q can take only integer values. Naively, $\theta_{\text{plaq}, x}$ adds up to zero, since each link angle appears with both signs. A nontrivial result is due to the fact that $\theta_{\text{plaq}, x}$ is thrown back to the interval $[-\pi, \pi)$.

In the case of open boundary conditions, the definitions of susceptibilities have to be adapted. In order to avoid large finite size effects, the sites with a distance less than l_0 from the open boundary are not taken into account, when computing the observables. Motivated by the rightmost part of eq. (4) we arrive at

$$\chi_{t, \text{open}} = \frac{1}{L_0 - 2l_0} \sum_{x_0=l_0}^{L_0-l_0-1} \langle \tilde{q}_{x_0}^2 \rangle + 2 \sum_{w=1}^{l_{\text{max}}} \frac{1}{L_0 - 2l_0 - w} \sum_{x_0=l_0}^{L_0-l_0-w-1} \langle \tilde{q}_{x_0} \tilde{q}_{x_0+w} \rangle . \quad (5)$$

3 Basic algorithms

As basic algorithm we use a hybrid of the Metropolis, the heat bath and the microcanonical overrelaxation algorithm. To a large extend, we follow section III of ref. [3]. Let us first discuss the updates of the site variables and then the updates of the gauge fields. In an elementary step of the algorithm we update the variable at a single site x , while keeping the gauge fields and the variables at all other sites fixed. The part of the action that depends on this site variable can be written as

$$\tilde{S}(z_x) = -\text{Re } z_x \bar{F}_x , \quad \text{where } F_x = 2N\beta \sum_{\mu} [\bar{\lambda}_{x,\mu} z_{x+\hat{\mu}} + \lambda_{x-\hat{\mu},\mu} z_{x-\hat{\mu}}] . \quad (6)$$

Note that the problem at this point is identical to the update of an $O(2N)$ invariant vector model with site variables of unit length. Instead of \bar{F}_x we would have to deal with the sum of the variables on the nearest neighbour sites. The microcanonical update keeps $\tilde{S}(z_x)$ fixed, while the new value of z_x has maximal distance from the old one. It is given by eq. (43a) of ref. [3]:

$$z'_x = 2 \frac{\text{Re } z_x \bar{F}_x}{|F_x|^2} F_x - z_x . \quad (7)$$

In addition to these updates, we have to perform updates that change the value of the action. To this end we implemented a heat bath algorithm that is applied to the subset of three of the $2N$ components of z_x , where we count both the real and the imaginary parts. The heat bath update is identical to the one used in the simulation of the $O(3)$ -Heisenberg model on the lattice or for the update of $SU(2)$ subgroups in the simulation of pure $SU(N)$ lattice gauge models [24, 25]. We run through all N complex components of z_x taking the real and the imaginary part of the component as first two components for the heat bath. The third component is randomly chosen among the real or imaginary parts of the remaining $N - 1$ components of z_x . Note that the CPU-time required by the microcanonical overrelaxation update is about one order of magnitude less than that for the heat bath update.

For fixed variables z the gauge fields can be updated independently of each other. The action reads

$$\tilde{S}_g(\lambda_{x,\mu}) = -\text{Re } \lambda_{x,\mu} \bar{f}_{x,\mu} , \quad \text{where } f_{x,\mu} = 2N\beta z_{x+\hat{\mu}} \bar{z}_x . \quad (8)$$

Here we perform a four hit Metropolis update, where the stepsize was chosen such that the acceptance rate is roughly 50%, and a microcanonical update, see eq. (43b) of [3].

3.1 Autocorrelation times

The performance of a Markov chain Monte Carlo algorithm is characterized by the autocorrelation time. There are different definitions of the autocorrelation time. These are based on the autocorrelation function. The autocorrelation function of an estimator A is given by

$$\rho_A(t) = \frac{\langle A_i A_{i+t} \rangle - \langle A \rangle^2}{\langle A^2 \rangle - \langle A \rangle^2} . \quad (9)$$

The modulus of the autocorrelation function is bounded from above by an exponentially decaying function. In practice one often finds that the autocorrelation function at large t is given by $\rho_A(t) \simeq c_A \exp(-t/\tau_{exp,A})$. The integrated autocorrelation time of the estimator A is given by

$$\tau_{int,A} = 0.5 + \sum_{t=1}^{\infty} \rho_A(t) . \quad (10)$$

The summation in eq. (10) has to be truncated at some finite t_{max} . Since $\rho_A(t)$ is falling off exponentially at large distances, the relative statistical becomes large at large distances. Therefore it is mandatory to truncate the summation at some point that is typically much smaller than the total length of the simulation. In the literature one can find various recommendations how this upper bound should be chosen. For example, Wolff [26] proposes to balance the statistical error with the systematic one that is due to the truncation of the sum.

4 Simulations with open boundary conditions

In order to keep the fraction of discarded sites small, it seems useful to chose $L_0 \gg L_1$. On the other hand, since the time needed for topological objects to diffuse to the centre of the lattice or back to the boundary increases with increasing L_0 , too large values of L_0 are not advisable. After performing preliminary simulations we decided to take $L_0 = 4L_1$ throughout. Furthermore we take $l_0 \approx 10\xi_{2nd}$ and $l_{max} = l_0$. For $N = 10$, using standard simulations and periodic boundary conditions, $\xi_{2nd} \approx 23$ can be reached [5]. Hence it is hard to demonstrate a clear advantage for open boundary conditions. Instead for $N = 21$ it is virtually impossible to go beyond $\xi_{2nd} \approx 6$ by using periodic boundary conditions and standard simulations. Therefore in the following we focus on our simulations for $N = 21$. We find that for $L_1 \gtrsim 16\xi_{2nd}$ finite L_1 effects can be ignored at the level of our statistical accuracy. We performed simulations for a large number of β -values, ranging from $\beta = 0.625$ up to 0.95. For each value of β , we performed 2×10^6 update cycles. For the larger values of β , we discarded 50000 update cycles at the beginning of the simulation. One update cycle consists of one sweep over all sites of the lattice using the heat bath algorithm, the 4 hit Metropolis update of the gauge fields, and finally n_{ov} sweeps using the overrelaxation algorithm for both the site variables and the gauge fields. We perform a measurement of the observables for each cycle. Autocorrelation times are quoted in units of these update cycles. The number of overrelaxation updates n_{ov} is chosen to be proportional to the correlation length. It increases from $n_{ov} = 3$ for $\beta = 0.625$ up to $n_{ov} = 28$ for $\beta = 0.95$. The second moment correlation length increases from $\xi_{2nd} = 2.2968(5)$ at $\beta = 0.625$ up to 18.2419(43) at $\beta = 0.95$.

Let us discuss the autocorrelation times of the topological susceptibility (4,5). For periodic boundary conditions, τ_{int} increases very rapid, compatible with exponential in the correlation length. Instead, for open boundary conditions, we first see an increase that is similar to that for periodic boundary conditions. The difference here can be attributed to the different definitions of the topological susceptibility (4,5). Then, for $\xi_{2nd} \gtrsim 5$ the autocorrelation time levels off for open boundary conditions.

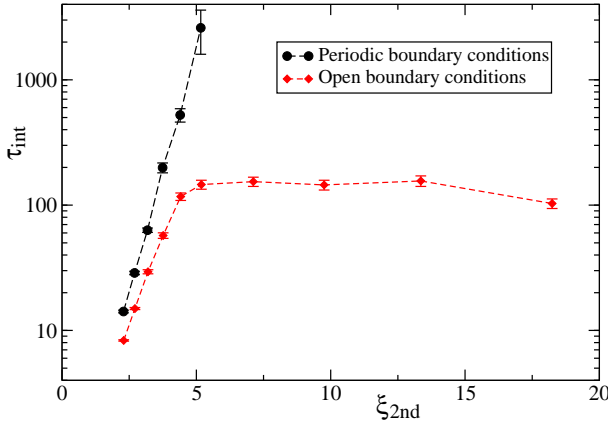


Figure 1. We plot the integrated autocorrelation time τ_{int} of the topological susceptibility for both periodic and open boundary conditions as a function of the second moment correlation length ξ_{2nd} for $N = 21$. Here τ_{int} is given in units of update cycles. For large ξ_{2nd} the effort for one update cycle is proportional to the number of overrelaxation sweeps n_{ov} . Hence, the plateau of τ_{int} corresponds to a dynamical critical exponent $z \approx 1$, taking single sweeps as unit of time.

The behaviour in the case of open boundary conditions can be explained along the lines of ref. [12]. For $\xi_{2nd} \lesssim 5$ changes of the topological charge are dominantly due to the creation and destruction of instantons in the bulk. Then for $\xi_{2nd} \gtrsim 5$ the diffusion from and to the boundaries completely dominates. This diffusion is not effected by the severe slowing down. Our numerical results for $N = 41$ confirm the conclusions drawn here for $N = 21$.

5 Parallel tempering in a line defect

In a parallel tempering simulation one introduces a sequence of N_t systems that differ in one parameter of the action. For each system there is a configuration $\{z, \lambda\}_t$. The tempering parameter might have a physical meaning. In statistical physics simulations this parameter is mostly the temperature. However it could also be a parameter that is introduced only for the sake of the simulation, as it is the case here. At one end of the sequence there is the system that we want to study. In our case this is a lattice with $L_0 = L_1$, periodic boundary conditions in both directions, and the coupling constant is the same for all links. For the system at the other end, it should be easy to sample the whole configuration space. Motivated by the success of the simulations with open boundary conditions, we use a system with a line defect to this end. Such a line defect is sketched in fig. 2. For $l_d = L_1$ we recover open boundary conditions.

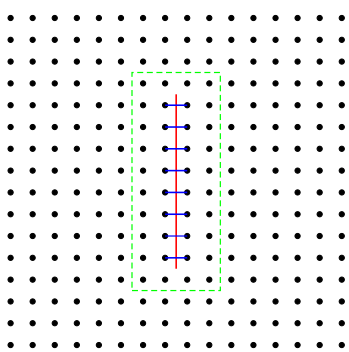


Figure 2. Sketch of a line defect. The red line indicates a line defect of length l_d . The coupling on the blue links is reduced or, in the extreme case, completely switched off. In our simulations we take for simplicity a linear interpolation: The couplings on the blue links are multiplied by $c_r(t) = 1 - t/(N_t - 1)$. The homogeneous system corresponds to $t = 0$, while for $t = N_t - 1$ the coupling along the defect line is completely eliminated. The green lines confine the area of a rectangle centred around the defect line. The size of the rectangle is $2l_i \times (l_d + 2l_i)$, where i gives the level. In our simulations $l_{i+1} = l_i/2$ for $i > 1$. For each update cycle at level i we perform n_{i+1} update cycles at level $i + 1$. At level $i = 0$ we sweep over the whole lattice. $l_1 = 2^m$, where m is an integer and $l_1 \approx \xi$. Furthermore $l_{i_{max}} = 1$.

In addition to updates of the individual systems there are exchanges of configurations between the systems. A swap of configurations $\{z, \lambda\}'_{t_1} = \{z, \lambda\}_{t_2}$, $\{z, \lambda\}'_{t_2} = \{z, \lambda\}_{t_1}$ between t_1 and t_2 is accepted

with the probability

$$A_{\text{swap}} = \min [1, \exp(-S_{t_2}(\{z, \lambda\}_{t_1}) - S_{t_1}(\{z, \lambda\}_{t_2}) + S_{t_1}(\{z, \lambda\}_{t_1}) + S_{t_2}(\{z, \lambda\}_{t_2}))] . \quad (11)$$

In our simulations we run from $t_1 = 0$ up to $t_1 = N_t - 2$ in steps of one, proposing to swap the configurations at t_1 and $t_2 = t_1 + 1$. The number of replica N_t is chosen such that the acceptance rate for the swap of configurations is larger than 30% for all t_1 . Note that S_{t_2} and S_{t_1} differ only on the defect line. Typically the swap of configurations is alternating with standard updates of the individual configurations. Typically, when the tempering parameter is homogeneous in space, a sweep over the whole lattice is performed. In contrast, here we temper in a defect that takes only a small fraction of the lattice. Therefore it is advisable to update only some part of the lattice that is centred around the defect. To this end, we introduce a sequence of rectangles of decreasing size, each associated with a level of our update scheme. For details see Fig. 2. In one update cycle, at a given level, we sweep over the rectangle, updating all N_t configurations: Once using the heat bath algorithm for the site variables and the 4 hit Metropolis update for the gauge fields. Then follow $n_{\text{ov},i}$ overrelaxation sweeps of the site variables and the gauge fields. For small i , $n_{\text{ov},i}$ is the same as for our simulations with open boundary conditions. For larger i , smaller values are taken. The update cycle at a given level is completed by a swap of configurations (11). We chose n_i such that for each level of the update scheme, roughly the same amount of CPU time is spent. The larger l_d , the more topological objects can be generated or destroyed. On the other hand, for increasing l_d , N_t has to be enlarged to keep the acceptance rate above 30%. Our numerical study shows that $l_d \approx \xi$ is the optimal choice. We perform a translation of the configuration for $t = 0$ after each swap. This way changes in the topology are injected at any location on the lattice and diffusion is not needed.

We performed simulations for $N = 10, 21$, and 41 and various values of β . Let us discuss the simulation for $N = 21$ and $\beta = 0.95$ in more detail. We used $l_d = 16$ and $N_t = 32$. The complete update cycle over all levels is characterized by $n_1 = 24$, $n_2 = n_3 = n_4 = 3$, and $n_5 = n_6 = 2$. The number of overrelaxation updates per cycle is 28, 14, 7, 7, 3, and 3 at levels 1, 2, 3, 4, 5, and 6, respectively. We find that the acceptance rate is about 81.4% for the pair $t = 0$ and 1. It drops to 39.4% for the pair $t = 26$ and 27. Then it increases again to 47.3% for the pair $t = 30$ and 31. The simulation, consisting of 50370 complete update cycles over all levels, took 25 days on a 4 core PC running with 8 threads. This is about the same CPU time that is used for the corresponding run with open boundary conditions. The error bar of the topological susceptibility is smaller by a factor of 2.3 compared with the simulation with open boundary conditions.

6 Physics results and comparison with the large N -expansion

Following ref. [27]

$$\frac{\xi_{2nd}}{\xi_{\text{exp}}} = \sqrt{\frac{2}{3}} + O(N^{-2/3}) . \quad (12)$$

Our results obtained for $N = 10, 21$ and 41 , which are plotted in Fig. 3 a are still quite far from this asymptotic value. Therefore we abstain from estimating the coefficient of the $O(N^{-2/3})$ corrections.

The product $\chi_t \xi^2$ should have a finite continuum limit. For the exponential correlation length the $1/N$ -expansion gives [28]

$$\chi_t \xi_{\text{exp}}^2 = \frac{3}{4\pi N} + O(N^{-5/3}) . \quad (13)$$

For the second moment correlation length a faster convergence with increasing N is obtained [27]

$$\chi_t \xi_{2nd}^2 = \frac{1}{2\pi N} \left(1 - \frac{0.38088...}{N} \right) + O(N^{-3}) . \quad (14)$$

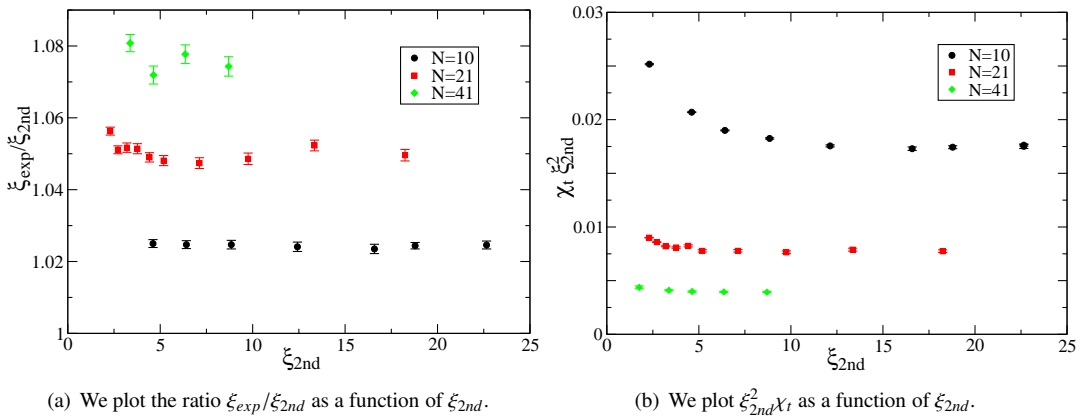


Figure 3. Physics results for $N = 10, 21$ and 41 .

In Fig. 3 b we plot $\xi_{2\text{nd}}^2 \chi_t$ as a function of $\xi_{2\text{nd}}$. Looking at the figure, the numerical data seem to converge nicely to the scaling limit. Corrections to scaling seem to be smaller for larger values of N . Taking simply the largest values of β for each N we get $\xi_{2\text{nd}}^2 \chi_t = 0.01737(8)$, $0.00767(5)$, and $0.00391(2)$ for $N = 10, 21$, and 41 , respectively. This can be compared with results quoted in the literature. For $N = 10$ one finds for example $\xi_{2\text{nd}}^2 \chi_t = 0.01719(10)(3)$ and $0.0175(3)$ in refs. [4, 5], respectively. For $N = 21$ one finds $\xi_{2\text{nd}}^2 \chi_t = 0.0080(2)$ and $0.0076(3)$ in refs. [4, 7], respectively. For $N = 41$ we find in ref. [7] the results $\xi_{2\text{nd}}^2 \chi_t = 0.0044(4)$ and $0.0036(4)$ for $\beta = 0.57$ and 0.6 , respectively. Our estimates are essentially consistent with those presented in the literature. In particular for large values of N , we improved the accuracy of the estimates. To see the effect of leading corrections, it is useful to multiply $\xi_{2\text{nd}}^2 \chi_t$ by $2\pi N$. Using our numbers, we get $1.091(5)$, $1.012(7)$, and $1.007(5)$ for $N = 10, 21$, and 41 , respectively. As already discussed in ref. [4] it is a bit puzzling that the numbers suggest a $1/N$ correction with the opposite sign as that of eq. (14).

7 Summary and conclusions

We have shown that the severe slowing down in the simulation of the lattice CP^{N-1} model can be avoided by using open boundary conditions in one of the directions. We studied parallel tempering in a line defect as an alternative. Our numerical results are encouraging. Focussing on the statistical error of the topological susceptibility, the simulation with open boundary conditions is outperformed by a factor of about 4. The crucial question is, of course, whether parallel tempering in a defect structure is helpful in simulations of lattice QCD. A more detail account of this study is given in [22].

Acknowledgments

I thank Stefan Schaefer for discussions. This work was supported by the Deutsche Forschungsgemeinschaft (DFG) under the grant No HA 3150/4-1.

References

- [1] A. D’Adda, M. Lüscher, P. Di Vecchia, Nucl. Phys. **B146**, 63 (1978)
- [2] E. Witten, Nuovo Cim. **A51**, 325 (1979)
- [3] M. Campostrini, P. Rossi, E. Vicari, Phys. Rev. **D46**, 2647 (1992)
- [4] L. Del Debbio, G.M. Manca, E. Vicari, Phys. Lett. **B594**, 315 (2004), hep-lat/0403001
- [5] J. Flynn, A. Jüttner, A. Lawson, F. Sanfilippo (2015), 1504.06292
- [6] E. Marinari, G. Parisi, Europhys. Lett. **19**, 451 (1992), hep-lat/9205018
- [7] E. Vicari, Phys. Lett. **B309**, 139 (1993), hep-lat/9209025
- [8] G.P. Engel, S. Schaefer, Comput. Phys. Commun. **182**, 2107 (2011), 1102.1852
- [9] A. Laio, G. Martinelli, F. Sanfilippo, JHEP **07**, 089 (2016), 1508.07270
- [10] M. Lüscher, S. Schaefer, JHEP **07**, 036 (2011), 1105.4749
- [11] M. Lüscher, S. Schaefer, Comput. Phys. Commun. **184**, 519 (2013), 1206.2809
- [12] G. McGlynn, R.D. Mawhinney, Phys. Rev. **D90**, 074502 (2014), 1406.4551
- [13] M. Bruno, S. Schaefer, R. Sommer (ALPHA), JHEP **08**, 150 (2014), 1406.5363
- [14] M. Bruno et al., JHEP **02**, 043 (2015), 1411.3982
- [15] Swendsen, Robert H. and Wang, Jian-Sheng, Phys.Rev.Lett. **57**, 2607 (1986)
- [16] Geyer, C. J., *Markov chain Monte Carlo maximum likelihood*, in *Computer Science and Statistics: Proc. of the 23rd Symposium on the Interface*, edited by Keramidas, E. M. (Interface Foundation, Fairfax Station, 1991), p. 156
- [17] Hukushima, Koji and Nemoto, Koji, J.Phys.Soc.Jpn. **65**, 1604 (1996), cond-mat/9512035
- [18] Earl, David J. and Deem, Michael W., Phys.Chem.Chem.Phys. **7**, 3910 (2005)
- [19] M. Baity-Jesi et al., Phys.Rev.B **88**, 224416 (2013), 1310.2910
- [20] N. Prokof’ev, B. Svistunov, Phys. Rev. Lett. **87**, 160601 (2001)
- [21] U. Wolff, Nucl. Phys. **B832**, 520 (2010), 1001.2231
- [22] M. Hasenbusch, Phys. Rev. **D96**, 054504 (2017), 1706.04443
- [23] B. Berg, M. Lüscher, Nucl. Phys. **B190**, 412 (1981)
- [24] N. Cabibbo, E. Marinari, Phys. Lett. **119B**, 387 (1982)
- [25] M. Creutz, Phys. Rev. **D21**, 2308 (1980)
- [26] U. Wolff (ALPHA), Comput. Phys. Commun. **156**, 143 (2004), [Erratum: Comput. Phys. Commun.176,383(2007)], hep-lat/0306017
- [27] M. Campostrini, P. Rossi, Phys. Lett. **B272**, 305 (1991)
- [28] M. Lüscher, Phys. Lett. **78B**, 465 (1978)